

Submitted to ApJ.

Tomographic Separation of Composite Spectra. IX. The Massive Close Binary HD 115071

Laura R. Penny¹

*Department of Physics and Astronomy
College of Charleston
Charleston, SC 29424;
pennyl@cofc.edu*

Douglas R. Gies²

*Center for High Angular Resolution Astronomy and
Department of Physics and Astronomy
Georgia State University, Atlanta, GA 30303;
gies@chara.gsu.edu*

John H. Wise³

*School of Physics
Georgia Institute of Technology
Atlanta, GA 30332;
jwise@astro.psu.edu*

D. J. Stickland, C. Lloyd

*Rutherford Appleton Laboratory
Chilton, Didcot, Oxon, OX11 0QX, United Kingdom;
ds@astro1.bnsc.rl.ac.uk, csl@ast.star.rl.ac.uk*

ABSTRACT

¹Guest Observer, Complejo Astronomico El Leoncito (CASLEO), San Juan, Argentina

²Guest Observer, Mount Stromlo and Siding Springs Observatories, Australia

³Current address: Department of Astronomy and Astrophysics, Pennsylvania State University, 532 Davey Laboratory, University Park, PA 16802

We present the first orbital elements for the massive close binary, HD 115071, a double-lined spectroscopic binary in a circular orbit with a period of 2.73135 ± 0.00003 days. The orbital semiamplitudes indicate a mass ratio of $M_2/M_1 = 0.58 \pm 0.02$ and yet the stars have similar luminosities. We used a Doppler tomography algorithm to reconstruct the individual component optical spectra, and we applied well known criteria to arrive at classifications of O9.5 V and B0.2 III for the primary and secondary, respectively. We present models of the *Hipparcos* light curve of the ellipsoidal variations caused by the tidal distortion of the secondary, and the best fit model for a Roche-filling secondary occurs for an inclination of $i = 48^\circ.7 \pm 2^\circ.1$. The resulting masses are $11.6 \pm 1.1 M_\odot$ and $6.7 \pm 0.7 M_\odot$ for the primary and secondary, respectively, so that both stars are very overluminous for their mass. The system is one of only a few known semi-detached, Algol-type binaries that contain O-stars. We suggest that the binary has recently emerged from extensive mass transfer (possibly through a delayed contact and common envelope process).

Subject headings: binaries: spectroscopic — stars: early-type — stars: evolution — stars: individual (HD 115071)

1. Introduction

The hot, massive star, HD 115071 (V961 Cen, LS 2998, HIP 64737), is found in the sky close to the open cluster, Stock 16 (Turner 1985), and is classified as O9.5 V by Houk & Cowley (1975) and B0.5 Vn by Garrison et al. (1977). The star is not a known visual binary (Mason et al. 1998) but early measurements by spectroscopists indicated it is radial velocity variable and a probable spectroscopic binary (Cruz-González et al. 1974; Conti et al. 1977). The proof of its binary nature came relatively recently in studies by Penny (1996) and Howarth et al. (1997). Both papers presented a cross-correlation analysis of a single, high dispersion, UV spectrum made with the *International Ultraviolet Explorer Satellite (IUE)* that demonstrated that the system is in fact a double-lined binary. Stickland & Lloyd (2001) measured the radial velocities of the components in this spectrum and proposed an orbital period of 2.73126 d based upon a light curve constructed from *Hipparcos* photometry. Lloyd & Stickland (2001) present a model of the light curve, and they argue that the system has evolved through Case A mass transfer (commencing during core H burning of the donor star).

The details and outcomes of Roche lobe overflow (RLOF) in massive binaries are still subjects of considerable debate (Wellstein et al. 2001), and thus, the orbital and physical

parameters of a system like HD 115071 are of great interest. Here we present the first double-lined orbital solution for the binary (§3) based upon new high quality optical spectra. We apply a version of the Doppler tomography algorithm (which we have used to good effect with UV spectra in prior papers in this series) to reconstruct the individual spectra of both components, from which we determine the spectral classifications, projected rotational velocities, and flux ratio (§4). We also present a light curve analysis constrained by the spectroscopic results that allows us to estimate the stellar masses (§5). These masses are much lower than expected, and we discuss the evolutionary implications in §6.

2. Observations and Reductions

Our spectra were obtained in two observing runs at different sites. The first set was obtained with the 2.15-m telescope of the Complejo Astronomico El Leoncito (CASLEO) and REOSC echelle spectrograph (on loan from the Institut d’Astrophysique, Universite de Liege, Belgium) during the period 1997 March 19 – 28. The REOSC spectrograph uses an echelle grating with 70 grooves mm^{-1} and blazed at 226434 Å together with a cross disperser grating of 400 grooves mm^{-1} blazed at 4000 Å. The detector was a TEK 1024×1024 CCD with $24\mu\text{m}$ square pixels used with a gain of $1.98 \text{ e}^-/\text{ADU}$ (read noise of 7.4 e^-). We used a $200\mu\text{m}$ slit that corresponds to $2''$ on the sky. This arrangement produced an echellogram from which we extracted 23 orders, spanning the range from 3575 to 5700 Å with a resolving power of $\lambda/\Delta\lambda = 13000$. We usually obtained 3 exposures of 660 s duration that were later co-added in software to improve the S/N (≈ 150 per pixel in the better exposed portions of the spectrum). Numerous bias, flat field, dark, and Th-Ar comparison images were obtained each night.

Our second observing run took place at the 74-inch telescope at Mount Stromlo Observatory over the period 1998 April 6 – 14. These spectra were made with the coude spectrograph using grating C (600 grooves per mm, blazed at 12500 Å in first order) in third order with a BG12 order sorting filter. The detector was a SITe CCD (D14) with $15 \mu\text{m}$ square pixels in a 4096×2048 format. This arrangement produced single order spectra that covered the range 3804 – 4220 Å with a reciprocal dispersion of 0.10 Å per pixel and a resolution element of 0.30 Å FWHM ($\lambda/\Delta\lambda = 13400$). Exposure times were usually 45 minutes, and the final spectra have a typical S/N = 160 per pixel in the continuum.

The spectra were reduced using standard routines in IRAF⁴. The MSO single-order

⁴IRAF is distributed by the National Optical Astronomy Observatories, which is operated by the Association of Universities for Research in Astronomy, Inc., under cooperative agreement with the National

spectra were extracted, calibrated, and flux rectified with the task *doslit*. The CASLEO echelle spectra were traced, extracted, and wavelength calibrated using the task *doecslit*, and the extracted orders were rectified to a unit continuum by fitting a high order spline function to line-free regions (using the task *continuum*). Finally the individual orders were linked together with the task *scombine*. Small amplitude irregularities related to the fitting of the echelle blaze function were evident in the continuum, and the same residual pattern was seen in all spectra made on a given night. We were able to remove most of the pattern by dividing the target spectrum by a correction spectrum formed from spectra of B-star, τ Sco, which was also observed each night. The correction spectrum was a smoothed version of the particular night’s τ Sco spectrum divided by a global average representation of this star’s stellar spectrum. The spectra from each run were then collected and transformed onto their respective heliocentric wavelength grids.

3. Radial Velocities and Orbital Elements

Our procedure for measuring radial velocities in *IUE* spectra (Penny et al. 1997) involves fitting Gaussians to the cross-correlation functions of the target spectrum with a narrow-lined reference spectrum. The optical spectra we consider here have many fewer stellar lines and much better S/N than the *IUE* spectra, so we revised our techniques accordingly. First, we fit each absorption feature separately rather than fitting the entire spectrum through one cross-correlation measurement. Secondly, we made the fit of the composite profiles using spectral templates rather than Gaussian functions (since the lines have shapes dominated by linear Stark broadening or rotational broadening and since some lines may contain weak blends). The templates were formed from spectra we obtained during each run of the star, HD 57682 (O9 IV; Walborn (1972)). This star is a reasonable match in classification to both components in HD 115071 (§4), but has narrower lines ($V \sin i = 33 \text{ km s}^{-1}$; Penny (1996)). The radial velocity of this star was measured by parabolic fitting of the line cores for lines in the list of Bolton & Rogers (1978), and we found an average radial velocity of 25.0 ± 0.5 and $26.0 \pm 1.1 \text{ km s}^{-1}$ from the CASLEO and MSO spectra, respectively. The averaged template spectra from each run were shifted by these values to place them in the rest frame. Next, we artificially broadened each template spectrum by convolution with a rotational broadening function to produce profiles that matched the spectral components of HD 115071 in the best separated quadrature spectra. We also used these resolved profiles to estimate the line depth ratio between the components. Once these fitting parameters were set, we determined the radial velocities of each component for a given line by a least-squares fit of the observed

profile with the coaddition of the two template profiles shifted in wavelength to obtain the best match. This approach provided good fits of the observed profiles for all but two cases (HJD 2,450,529.792 and 2,450,531.755) where the line depth ratio appeared to be reversed.

We used this technique to measure radial velocities for the strongest lines in the spectrum, specifically H I $\lambda\lambda$ 3835, 3889, 3970, 4101, 4340, 4861, He I $\lambda\lambda$ 3819, 4009, 4026, 4121, 4143, 4387, 4471, 4921, 5015, He II λ 4686, and Si IV λ 4089. There was no evidence of systematic line-to-line differences in the radial velocity measurements, and so no line specific corrections were applied. The radial velocities from all the available lines were averaged together after deletion of any very discrepant measurements. Finally, we made small adjustments to these averages based on measurements of the strong interstellar Ca II $\lambda\lambda$ 3933, 3968 lines. An interstellar spectrum was formed by extracting the mean spectrum in the immediate vicinity of each interstellar absorption line. (We made Gaussian fits of the interstellar Ca II profiles in the extracted spectra, and we found the radial velocity was -17.0 ± 0.2 and -16.0 ± 0.2 km s $^{-1}$ for the mean CASLEO and MSO spectra, respectively.) We then cross correlated this spectrum with each individual spectrum to measure any small deviations in our wavelength calibration (generally < 3 km s $^{-1}$), and these small corrections were applied to the mean velocities. Table 1 lists the heliocentric dates of mid-observation, orbital phase, and for each component, the mean radial velocity, the standard deviation of the mean, the observed minus calculated residual from the orbital fit, and the number of lines used in the mean. Table 1 also gives the radial velocities from the single *IUE* spectrum measured by Stickland & Lloyd (2001) (adjusted for the ISM velocity on the MSO system).

Stickland & Lloyd (2001) and Lloyd & Stickland (2001) found that the *Hipparcos* light curve was best fit with a double sine, ellipsoidal variation for an orbital period $P = 2.73126 \pm 0.00009$ d. We found that this period also agreed reasonably well with our radial velocity data. We used the non-linear, least-squares fitting program of Morbey & Brosterhus (1974) to solve for the period and other orbital elements for the primary (the more luminous and massive star) and secondary components separately, and this yielded period estimates of 2.73149 ± 0.00007 and 2.73138 ± 0.00015 d, respectively. We made one additional calculation of the period by dividing the difference between the best fit time of the *Hipparcos* photometry maximum and our spectroscopically determined time of quadrature by the closest integral number of cycles, and this led to a period of 2.73130 ± 0.00004 d. We adopted the error weighted mean of these three estimates for our working value of the period, $P = 2.73135 \pm 0.00003$ d.

We fixed this period and then fit for the remaining orbital elements independently for both components. The fitted epoch of primary maximum velocity, T_0 , was the same within errors for both solutions, and so we applied the mean value to fits of both components.

Eccentric solutions produced estimates of eccentricity consistent with a value of zero, and our final solutions in Table 2 assume circular motion. The observed and calculated radial velocity curves appear in Figure 1. The only major discrepancies occur in the *IUE* measurements (not used in the solution), both of which are $\approx 38 \text{ km s}^{-1}$ above the predicted curve. Note that in the case of the primary, the *IUE* velocity falls well above the maximum for the entire curve, so the mismatch cannot be due to an incorrect orbital phase for example. The systematic difference may be related to line formation at different heights in an expanding atmosphere or orbital motion about a distant, unseen, tertiary star.

4. Tomographic Reconstruction

We used the Doppler tomography algorithm described by Bagnuolo et al. (1994) to reconstruct the individual primary and secondary spectra independently from the CASLEO and MSO spectra. We took the radial velocity shifts for each component from the orbital solutions in Table 2, then the reconstruction was run for 50 iterations with a gain of 0.8 (the results are insensitive to both parameters). The reconstructed spectra are plotted in in Figure 2 in a format similar to that used in the spectral atlas of Walborn & Fitzpatrick (1990). The reconstructions from the MSO spectra are shown just above those from the CASLEO spectra (in the short wavelength portion of Fig. 2), and there is good agreement between these two sets of spectra.

We compared the reconstructed spectra with the spectrum standards in the atlas of Walborn & Fitzpatrick (1990) to determine the spectral classifications of the components. The strengths of the He I $\lambda\lambda 4026, 4143, 4387$ lines relative to those of He II $\lambda\lambda 4200, 4541$ are all consistent with a spectral type of O9.5 for the primary. The ratio of the Si IV $\lambda\lambda 4088, 4116$ lines to the nearby He I $\lambda\lambda 4121, 4143$ features indicate a main sequence class, as does the relatively strong He II $\lambda 4686$ to He I $\lambda 4713$ ratio. Thus, we classify the primary as type O9.5 V, and we compare its spectrum in Figure 2 to that of HD 93027, which is given as the standard of this class in Walborn & Fitzpatrick (1990).

The secondary, on the other hand, has features indicating a cooler temperature and later type. The ratio of Si III $\lambda 4552$ to Si IV $\lambda 4088$ has a good match in the interpolated type B0.2 introduced by Walborn & Fitzpatrick (1990). The relative strength of the Si IV $\lambda\lambda 4088, 4116$ lines compared to the neighboring He I $\lambda\lambda 4121, 4143$ features clearly leads to a luminosity class III. Figure 2 illustrates the good agreement between the spectrum of the secondary and that of HD 108639 that Walborn & Fitzpatrick (1990) use as a standard for type B0.2 III. The C III $\lambda\lambda 4070, 4650$ blends appear to be somewhat weaker in the secondary’s spectrum than in the standard spectrum (evidence, perhaps, of CNO-processed gas in the secondary’s

photosphere).

The two spectral standards, HD 93027 and HD 108639, provided us with the means to estimate the visual flux ratio, $r = F_2/F_1$, by matching the line depths in the reconstructed spectra with those in the standards. This was done by aligning the reconstructed and standard spectra, adjusting for differences in the placement of the continuum, Gaussian smoothing of the spectra to eliminate differences in projected rotational velocity and instrumental broadening, and then finding a best fit line ratio that allocates a proportion of flux to each component to best match the line depths. We found $r = 1.04 \pm 0.06$ and 1.08 ± 0.08 for the MSO and CASLEO reconstructions, respectively.

Finally, we used the profiles in the reconstructed spectra to estimate the projected rotational velocities of the components. We focused on the Si IV $\lambda 4088$ profile for this purpose since it represents the strongest metallic line (intrinsically narrow) in the range covered by the MSO spectra. Our procedure involved calculating a grid of rotational broadening functions for a linear limb darkening law (Wade & Rucinski 1985; Gray 1992) and then convolving an observed narrow-lined spectrum with these broadening functions. We compared the spectral reconstructions from the MSO spectra with broadened versions of MSO spectra of the narrow-lined stars HD 53682 (O9 IV) and τ Sco (B0.2 V). The best fitting profile matches were made with $V \sin i = 101 \pm 10$ and 132 ± 15 km s⁻¹ for the primary and secondary, respectively. These agree within errors with estimates from the *IUE* observation (Penny 1996; Howarth et al. 1997; Lloyd & Stickland 2001).

5. Light Curve Analysis and Masses

Lloyd & Stickland (2001) presented an analysis of the *Hipparcos* light curve (Perryman 1997), and here we update their work by restricting a number of the fitting parameters based upon the new spectroscopic results. We used the light curve synthesis code GENSYN (Mochnacki & Doughty 1972) to produce model *V*-band differential light curves (almost identical to differential *Hipparcos* *Hp* magnitudes for hot stars). The orbital parameters were taken from the spectroscopic solution, and the physical parameters were estimated from the spectral classifications of the stars. We first estimated the stellar temperature and gravity according to the spectral classification calibration of Howarth & Prinja (1989) for the primary ($T_{\text{eff } 1} = 32$ kK, $\log g_1 = 3.9$), and for the secondary, we used data for comparable stars in the compilation of Underhill & Doazan (1982) ($T_{\text{eff } 2} = 29$ kK, $\log g_2 = 3.6$). We then determined the physical fluxes and limb darkening coefficients from tables in Kurucz (1994) and Wade & Rucinski (1985), respectively. We also used the Kurucz flux models to transform our observed flux ratio based upon the relative line depths into a *V*-band flux ratio (Penny et

al. 1997). The MSO spectra are centered at 4009 Å, and the transformation yields a V -band flux ratio, $F_2/F_1 = 1.05 \pm 0.06$. The comparison of line depths in the CASLEO spectra was made over the available range in the standard spectrum from Walborn & Fitzpatrick (1990) (centered at 4350 Å), and the resulting V -band flux ratio is $F_2/F_1 = 1.09 \pm 0.06$. We used the average value, $F_2/F_1 = 1.07 \pm 0.06$, in the light curve analysis. The theoretical and observed flux ratios together yield an approximate estimate of the ratio of stellar radii, $R_2/R_1 = 1.12 \pm 0.03$. Each trial run of GENSYN was set by two independent parameters, the system inclination i and secondary’s radius relative to the critical Roche-filling case (with the primary radius set so that the orbital average flux ratio matched the observed flux ratio).

The observed light curve (Fig. 3) is a double-sine wave caused by tidal distortion in the stars. Since the stars have similar radii but the secondary has a much lower mass (§3), the secondary must be much closer to filling its critical Roche radius, so that the tidal generation of the light curve is due mainly to the distortion of the secondary. The amplitude of the photometric variation is proportional to the degree of tidal distortion (how close the secondary comes to filling its Roche volume) and to the sine of the inclination (maximal effect for $i = 90^\circ$). Our first fit of the light curve assumed that the secondary completely fills its Roche volume, so this solution corresponds to the case of minimum inclination (and maximum masses). The best fit for this semi-detached configuration is made with an inclination, $i = 48.7 \pm 2.1$, and this fit is shown as the solid line in Figure 3. The error in the inclination results from two sources, the variation in the χ^2 residuals of the fit with parameter i and the change in the solution introduced by the uncertainty in the flux ratio. The root mean square of the residuals from the best fit is 0.019 mag, which is approximately $1.7\times$ larger than the errors quoted in the *Hipparcos* catalog, and so some other kind of photometric variation may exist that is unrelated to orbital phase.

Note that it is possible to obtain fits with a lower inclination if the flux ratio constraint is abandoned. For example, we found that if we assumed a contact configuration in which both stars fill their Roche volumes, then we could make a satisfactory fit of the light curve with $i = 38^\circ$. However, we rule out this model because it predicts a flux ratio, $F_2/F_1 = 0.52$, that is far below the limits established from the spectra of the components.

Models with a smaller secondary and less tidal distortion require a higher inclination to match the observations (yielding lower masses), but these solutions are less satisfactory for two reasons. First, higher inclination solutions generally yield light curves with less ellipsoidal variation but some evidence of eclipses. We show one example in Figure 3 for an inclination $i = 60^\circ$ and a secondary volume radius of $R_2/R_\odot = 5.6$ ($\approx 90\%$ of the critical Roche radius). Eclipses as subtle as those shown in Figure 3 are probably not ruled out by the *Hipparcos* photometry, but models with $i > 62^\circ$ show eclipses that are clearly inconsistent with the

Hipparcos light curve. Secondly, the projected rotational velocities predicted by underfilling models with synchronous rotation are much smaller than the observed values. All the known binaries containing O-stars with periods this short have circular orbits (Mason et al. 1998), and we expect that such close systems have attained synchronous rotation as well (Claret & Cunha 1997). The predicted projected rotational velocities are $V \sin i = 92$ and 109 km s^{-1} for the primary and secondary, respectively, in the Roche-filling model, in agreement within errors with the observed values (§4). However, the match is worse in higher inclination models ($V \sin i = 81$ and 94 km s^{-1} , respectively, for the $i = 60^\circ$ model illustrated in Fig. 3). Thus, we prefer the secondary Roche-filling model, and we list in Table 3 the corresponding stellar parameters. The system absolute magnitude in this model is $M_V = -4.57$, and, for $V = 7.94$ and $E(B - V) = 0.50$ (Turner 1985), we estimate a distance of $1.5 \pm 0.2 \text{ kpc}$ (smaller than but comparable to the distance of 1.9 kpc for the cluster Stock 16; Turner (1985)).

6. Discussion

The first striking result from our analysis is the very low mass we find for both components. The stars have temperatures and luminosities that are associated with masses of 18 and $15M_\odot$ for the primary and secondary, respectively, in the single star evolutionary tracks calculated by Schaller et al. (1992). (These estimates would be slightly reduced using evolutionary models that include rotation; Heger & Langer (2000), Meynet & Maeder (2000).) The secondary, in particular, has a luminosity characteristic of a star more than twice as massive than we find (Table 3).

The second remarkable fact is that the secondary star has a spectral classification indicating it has evolved away from the main sequence. Thus, HD 115071 presents the classical “Algol paradox” that the lower mass component is the more evolved one, and we suggest the same solution of the paradox holds here as well, i.e., that the evolved component was originally the more massive object, but suffered significant mass transfer to its neighbor.

There are only a small number of O-stars that are known to be members of interacting binaries, and we compare in Table 4 the properties of the components in HD 115071 with those of the four other known semi-detached binaries that contain O-type stars (Hilditch & Bell 1987; Harries & Hilditch 1998). We excluded from this list contact or over-contact systems and those binaries in which both components are evolved (Vanbeveren et al. 1998). All the systems in Table 4 share a number of common properties: the mass donor appears as an evolved star, the donor star is overluminous for its mass, the donor fills its Roche volume, and the mass gainer is a late O-type, main sequence star. It is remarkable that

all the donor stars have comparable luminosity, $\log L/L_{\odot} \approx 4.5$, despite their wide range in mass and radius. Evolutionary models generally predict that the post-RLOF luminosity of the donor is comparable to its zero age main sequence (ZAMS) luminosity (Vanbeveren et al. 1998; Wellstein et al. 2001), and so these donors probably began life as B0 V stars with masses in the range $14 - 20M_{\odot}$. Since the donors were originally the more massive component, the gainers were probably also B-type stars that were promoted to their current O-type status through mass transfer. It is also curious that no semi-detached systems are known with primaries earlier than type O8 V. Either this stage is extremely rapid in more massive systems or the donor stars take on a different appearance than they do in Algol-type systems (perhaps as a O-star plus Wolf-Rayet star binary; Vanbeveren et al. (1998)).

Evolutionary models give us some guidance about the initial masses in HD 115071. de Loore & Vanbeveren (1994) give a relationship between the final, post-RLOF mass and the initial ZAMS mass, and this yields an estimate of $14.8M_{\odot}$ for the initial mass of the donor star. If we further assume that 50% of the donor’s mass loss was accreted by gainer and the rest lost from the system (Meurs & van den Heuvel 1989; de Loore & Vanbeveren 1994), then the original total mass was $22.4M_{\odot}$ and the original gainer mass was $7.6M_{\odot}$. Thus, the system probably began with a relatively low mass ratio, $M_g/M_d \approx 0.5$.

The theoretical models of binary evolution by Wellstein et al. (2001) offer some guidance in the interpretation of our results. Wellstein et al. (2001) describe the evolution of several very close systems that begin RLOF during core H-burning (Case A). Their models suggest that a mass reversal similar to what we find in HD 115071 can occur in Case A, but the resulting systems generally have a much wider orbit and more extreme mass ratio. Another possibility is that the system began RLOF after completion of core H burning (Case B). The initial period would have been much larger, but the system then shrunk to its current dimensions during a common envelope phase in which the donor’s envelope would have been ejected from the system. This would explain the current mass and luminosity of the donor star, but it does not account for the huge overluminosity of the contemporary primary star, which is the most overluminous star of any of the gainers in Table 4. Wellstein et al. (2001) point out one other hybrid scheme they call “delayed contact” in which mass transfer begins conservatively until the donor develops a convective envelope and the binary enters the common envelope stage. This scenario would explain the observed low mass of the donor and the short orbital period, and the overluminosity of the gainer would result from compression and/or mixing related to mass accretion.

The best fit of the light curve suggests that the secondary donor star is Roche-filling, and so the system may still be experiencing active mass transfer. Observations of any H α emission (Thaller 1997) or IR excess (Gehrz et al. 1995) would provide valuable clues

about the mass loss and/or mass transfer processes that might be occurring presently in this exceptional binary system.

We thank the staffs of CASLEO and MSO for their assistance in making these observations. We are grateful to Norbert Langer for comments on the evolutionary state of the binary. Institutional support for L.R.P. has been provided from the College of Charleston School of Sciences and Mathematics. Additional support for L.R.P. was provided by the South Carolina NASA Space Grant Program and NSF grant AST-9528506. Institutional support for D.R.G. has been provided from the GSU College of Arts and Sciences and from the Research Program Enhancement fund of the Board of Regents of the University System of Georgia, administered through the GSU Office of the Vice President for Research. We gratefully acknowledge all this support.

REFERENCES

- Bagnuolo, W. G., Jr., Gies, D. R., Hahula, M. E., Wiemker, R., & Wiggs, M. S. 1994, *ApJ*, 423, 446
- Bolton, C. T., & Rogers, G. L. 1978, *ApJ*, 222, 234
- Claret, A., & Cunha, N. C. S. 1997, *A&A*, 318, 187
- Conti, P. S., Leep, E. M., & Lorre J. J. 1977, *ApJ*, 214, 759
- Cruz-González, C., Recillas-Cruz, E., Costero, R., Peimbert, M., & Torres-Peimbert, S. 1974, *Revista Mexicana Astr. Astrof.*, 1, 211
- de Loore, C., & Vanbeveren, D. 1994, *A&A*, 292, 463
- Garrison, R. F., Hiltner, W. A., & Schild, R. E. 1977, *ApJS*, 35, 111
- Gehrz, R. D., et al. 1995, *ApJ*, 439, 417
- Gray, D. F. 1992, *The Observation and Analysis of Stellar Photospheres* (2nd ed.) (Cambridge: Cambridge Univ. Press)
- Harries, T. J., & Hilditch, R. W. 1998, in *Boulder-Munich II: Properties of Hot, Luminous Stars* (ASP Conf. Ser. Vol. 131), ed. I. D. Howarth (San Francisco: ASP), 401
- Harries, T. J., Hilditch, R. W., & Hill, G. 1997, *MNRAS*, 285, 277
- Harries, T. J., Hilditch, R. W., & Hill, G. 1998, *MNRAS*, 295, 386
- Heger, A., & Langer, N. 2000, *ApJ*, 544, 1016
- Hilditch, R. W., & Bell, S. A. 1987, *MNRAS*, 229, 529
- Houk, N., & Cowley, A. P. 1975, *Catalogue of two dimensional spectral types for the HD stars*, Vol. 1 (Ann Arbor: Univ. Michigan)
- Howarth, I. D., & Prinja, R. K. 1989, *ApJS*, 69, 527
- Howarth, I. D., Siebert, K. W., Hussain, G. A. J., & Prinja, R. K. 1997, *MNRAS*, 284, 265
- Kurucz, R. L. 1994, *Solar Abundance Model Atmospheres for 0, 1, 2, 4, 8 km/s*, Kurucz CD-ROM No. 19 (Cambridge, MA: Smithsonian Astrophysical Obs.)
- Lloyd, C., & Stickland, D. J. 2001, *A&A*, 370, 1026

- Lorenz, R., Mayer, P., & Drechsel, H. 1994, *A&A*, 291, 185
- Mason, B. D., Gies, D. R., Hartkopf, W. I., Bagnuolo, W. G., Jr., ten Brummelaar, T., & McAlister, H. A. 1998, *AJ*, 115, 821
- Meurs, E. J. A., & van den Heuvel, E. P. J. 1989, *A&A*, 226, 88
- Meynet, G., & Maeder, A. 2000, *A&A*, 361, 101
- Mochmacki, S. W., & Doughty, N. A. 1972, *MNRAS*, 156, 51
- Morbey, C. L., & Brosterhus, E. B. 1974, *PASP*, 86, 455
- Penny, L. R. 1996, *ApJ*, 463, 737
- Penny, L. R., Gies, D. R., & Bagnuolo, W. G., Jr. 1997, *ApJ*, 483, 439
- Perryman, M. A. C. 1997, *The Hipparcos and Tycho Catalogues*, ESA SP-1200 (ESA/ESTEC, Noordwijk)
- Schaller, G., Schaerer, D., Meynet, G., & Maeder, A. 1992, *A&AS*, 96, 269
- Stickland, D. J., & Lloyd, C. 2001, *Observatory*, 121, 1
- Thaller, M. L. 1997, *ApJ*, 487, 380
- Turner, D. G. 1985, *ApJ*, 292, 148
- Underhill, A., & Doazan, V. (eds.) 1982, *B Stars With and Without Emission Lines* (NASA SP-456) (Washington, DC: NASA)
- Wade, R. A., & Rucinski, S. M. 1985, *A&AS*, 60, 471
- Walborn, N. R. 1972, *AJ*, 77, 312
- Walborn, N. R., & Fitzpatrick, E. L. 1990, *PASP*, 102, 379
- Wellstein, S., Langer, N., & Braun, H. 2001, *A&A*, 369, 939
- Vanbeveren, D., van Rensbergen, W., & de Loore, C. 1998, *The Brightest Binaries* (Dordrecht: Kluwer)

Fig. 1.— The radial velocity measurements (*primary* – *filled circles*; *secondary* – *open circles*) and orbital solution (*solid lines*) plotted against orbital phase. Phase zero corresponds to the time of primary maximum radial velocity. The two plus marks show the *IUE* measurements that were not used in the solution.

Fig. 2.— A comparison of the reconstructed MSO spectra (*above*) and CASLEO spectra (*below*) of the primary and secondary with spectra of the same classifications from Walborn & Fitzpatrick (1990). All the spectra were Gaussian smoothed to a nominal resolution of 1.2 Å FWHM for consistent line broadening.

Fig. 3.— The *Hipparcos* light curve plotted against spectroscopic orbital phase. The solid line shows the predicted curve for a secondary Roche-filling model with $i = 48^\circ.7$, while the dashed line represents the prediction for an under-filling model with $i = 60^\circ$.

Table 1. Radial Velocity Measurements

HJD (-2,400,000)	Orbital Phase	V_1 (km s ⁻¹)	σ_1 (km s ⁻¹)	$(O - C)_1$ (km s ⁻¹)	n_1	V_2 (km s ⁻¹)	σ_2 (km s ⁻¹)	$(O - C)_2$ (km s ⁻¹)	n_2
44487.472	0.921	104.4	...	34.0	...	-151.6	...	41.2	...
50526.858	0.057	80.5	6.2	3.6	17	-189.6	2.2	14.5	12
50527.780	0.394	-117.3	3.5	-4.2	17	131.3	6.8	5.3	17
50528.845	0.784	-1.8	5.5	1.2	17	-47.6	5.1	17.7	16
50529.792	0.131	52.3	2.7	3.7	13	-160.3	2.1	-5.4	14
50530.777	0.491	-122.8	7.1	13.5	17	182.1	7.8	15.6	16
50531.755	0.849	32.6	6.3	-5.4	17	-148.0	4.6	-11.5	17
50532.783	0.226	-0.3	6.0	9.4	16	-28.2	7.7	25.5	16
50533.754	0.581	-125.5	4.4	-3.0	17	159.1	8.4	16.8	17
50535.766	0.318	-82.8	4.7	-10.8	15	43.4	3.1	-11.2	12
50910.125	0.378	-98.5	1.7	7.3	9	107.6	2.3	-5.7	10
50911.086	0.730	-22.1	2.6	18.1	9	-31.6	5.6	-31.0	10
50911.171	0.761	-29.4	0.4	-10.4	6	-34.3	5.4	3.2	10
50916.213	0.607	-119.0	4.1	-6.4	10	122.8	5.6	-2.3	10
50916.990	0.891	58.8	2.5	-0.2	9	-166.8	2.4	6.2	9
50917.116	0.938	73.9	4.6	-1.5	10	-204.6	3.5	-3.1	9
50917.257	0.989	79.8	5.4	-3.7	10	-220.4	4.4	-4.8	10
50917.971	0.250	-26.8	1.8	-0.1	8	-28.0	4.9	-3.8	9
50918.112	0.302	-59.8	3.8	2.0	8	23.6	2.7	-13.4	9
50918.249	0.352	-105.3	3.2	-13.0	10	77.5	2.4	-12.4	9

Table 2. Circular Orbital Elements

Element	Value
P (days)	2.73135 (3)
T_0 (HJD-2,400,000)	50734.286 (11)
K_1 (km s ⁻¹)	110.1 (28)
K_2 (km s ⁻¹)	191.4 (48)
$V_{0\ 1}$ (km s ⁻¹)	-26.4 (19)
$V_{0\ 2}$ (km s ⁻¹)	-24.6 (32)
$m_1 \sin^3 i$ (M_\odot)	4.94 (40)
$m_2 \sin^3 i$ (M_\odot)	2.84 (26)
$a_1 \sin i$ (R_\odot)	5.94 (15)
$a_2 \sin i$ (R_\odot)	10.32 (26)
r.m.s. ₁ (km s ⁻¹) . . .	8.4
r.m.s. ₂ (km s ⁻¹) . . .	14.2

Note. — Numbers in parentheses give the error in the last digit quoted.

Table 3. Stellar Properties

Property	Primary	Secondary
Spectral Classification . . .	O9.5 V	B0.2 III
Relative flux $F/F_1(5470\text{\AA})$	1.0	1.07 ± 0.06
$V \sin i$ (km s ⁻¹)	101 ± 10	132 ± 15
T_{eff} (kK)	32 ± 2	29 ± 1.5
M/M_\odot	11.6 ± 1.1	6.7 ± 0.7
R/R_\odot	6.5 ± 0.2	7.2 ± 0.2
$\log g$	3.88 ± 0.01	3.55 ± 0.01
$\log L/L_\odot$	4.60 ± 0.14	4.52 ± 0.12

Table 4. Semi-Detached OB-Star Binaries

Name	P (d)	Pri. Type	Sec. Type	M_P (M_\odot)	M_S (M_\odot)	$\log L_P/L_\odot$	$\log L_S/L_\odot$	Ref.
HD 115071 = V961 Cen	2.73	O9.5 V	B0.2 III	11.6 ± 1.1	6.7 ± 0.7	4.60 ± 0.14	4.52 ± 0.12	1
HD 209481 = LZ Cep ..	3.07	O8.5	O9.5	15.1 ± 0.4	6.3 ± 0.2	4.90 ± 0.03	4.65 ± 0.03	2
BD+66° 1521 = XZ Cep	5.10	O9.5 V	B1 III	15.8 ± 0.4	6.4 ± 0.3	4.58 ± 0.04	4.48 ± 0.03	3
HD 106871 = AB Cru .	3.41	O8 V	B0.5	19.8 ± 1.0	7.0 ± 0.7	5.21 ± 0.03	4.58 ± 0.03	4
HD 190967 = V448 Cyg	6.52	O9.5 V	B1 II-Ib	25.2 ± 0.7	14.0 ± 0.7	4.54 ± 0.04	4.66 ± 0.06	3

Note. — References: (1) this paper, (2) Harries et al. (1998), (3) Harries et al. (1997), (4) Lorenz et al. (1994).

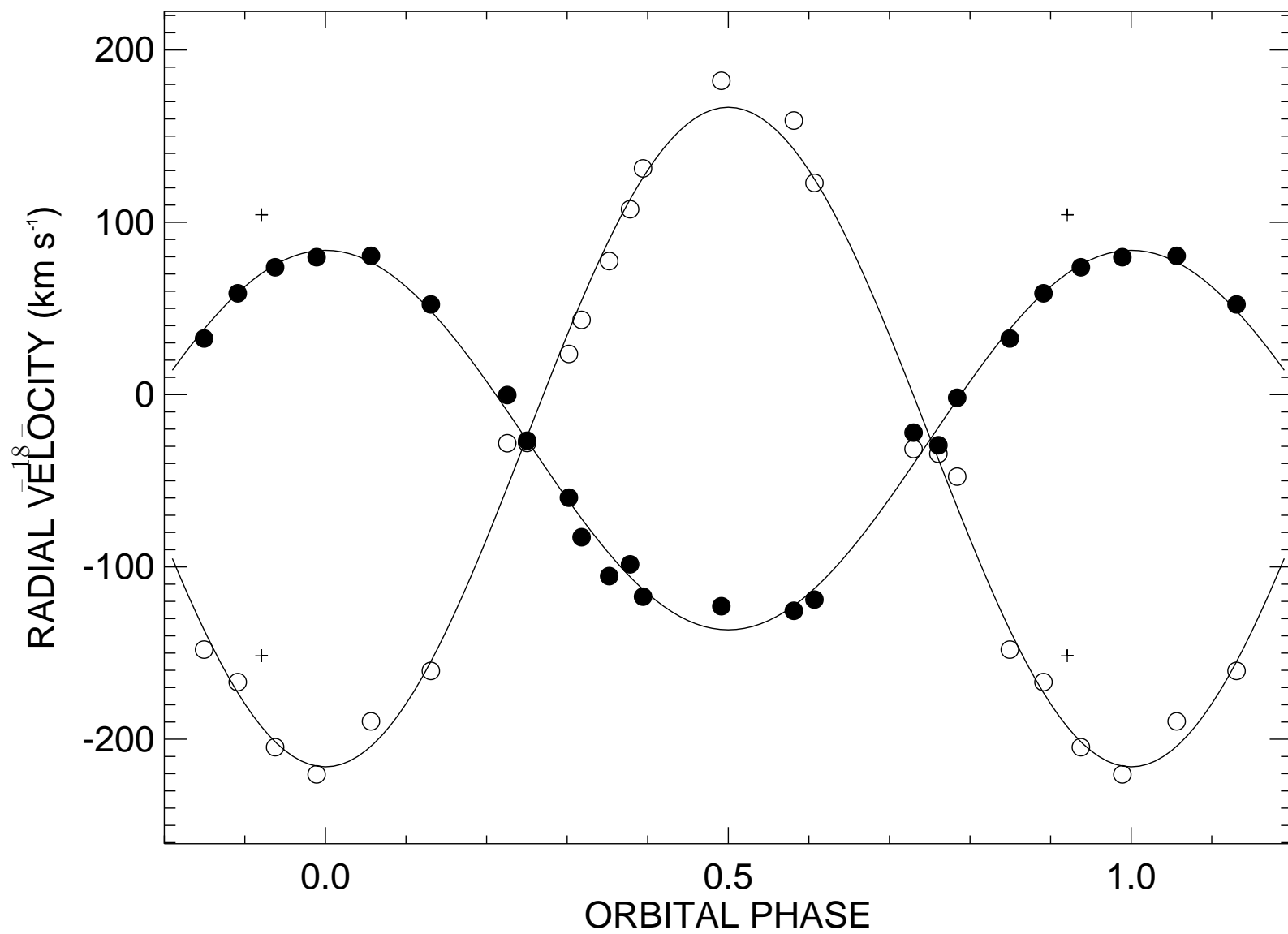


Fig. 1.—

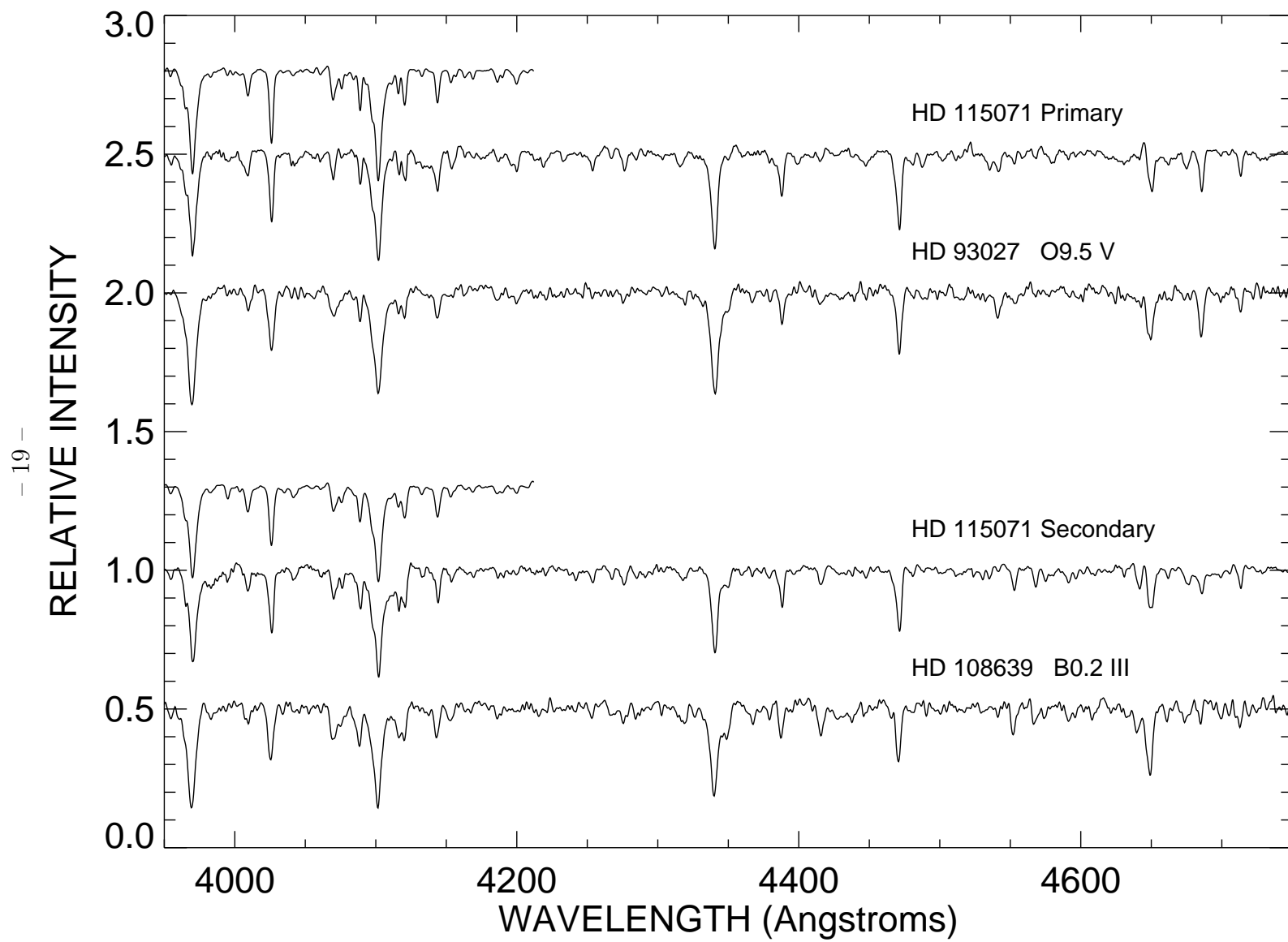


Fig. 2.—

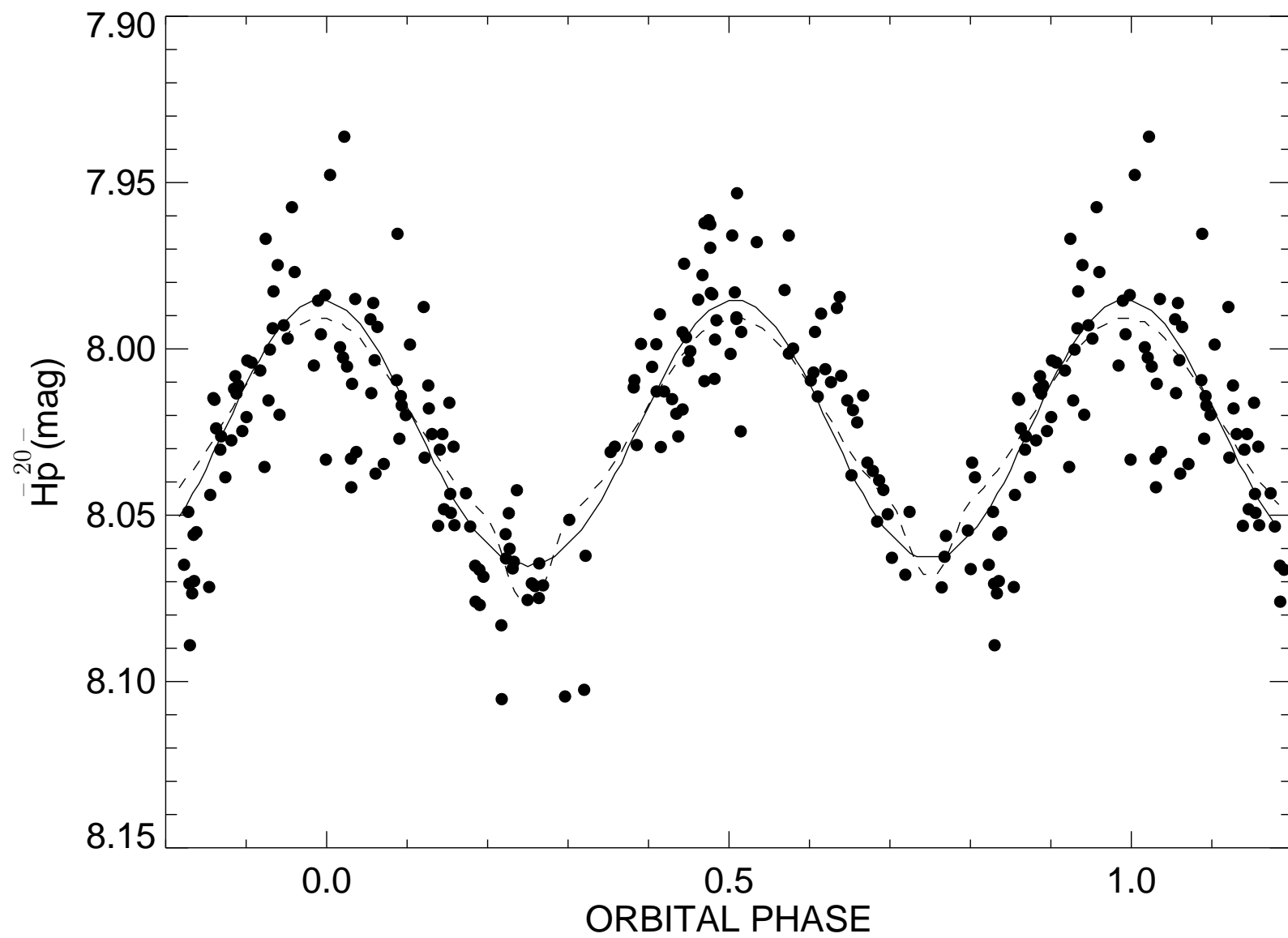


Fig. 3.—